Compact Dielectric Wall Accelerator Development For Intensity Modulated Proton Therapy And Homeland Security Applications

Y. -J. Chen, G. J. Caporaso, G. Guethlein, S. Sampayan, G. Akana, R. Anaya, D. Blackfield, E. Cook, S. Falabella, Ed. Gower, J. Harris, S. Hawkins, B. Hickman, C. Holmes, A. Horner, S. Nelson, A. Paul, D. Pearson, B. Poole, R. Richardson, D. Sanders, J. Stanley, J. Sullivan, L. Wang, J. Watson, J. Weir

June 25, 2009

Disclaimer

This document was prepared as an account of work sponsored by an agency of the United States government. Neither the United States government nor Lawrence Livermore National Security, LLC, nor any of their employees makes any warranty, expressed or implied, or assumes any legal liability or responsibility for the accuracy, completeness, or usefulness of any information, apparatus, product, or process disclosed, or represents that its use would not infringe privately owned rights. Reference herein to any specific commercial product, process, or service by trade name, trademark, manufacturer, or otherwise does not necessarily constitute or imply its endorsement, recommendation, or favoring by the United States government or Lawrence Livermore National Security, LLC. The views and opinions of authors expressed herein do not necessarily state or reflect those of the United States government or Lawrence Livermore National Security, LLC, and shall not be used for advertising or product endorsement purposes.

Compact Dielectric Wall Accelerator Development For Intensity Modulated Proton Therapy And Homeland Security Applications*

Y.-J. Chen[a], G. J. Caporaso[a], G. Guethlein[a], S. Sampayan[a], G. Akana[a],
R. Anaya[a], D. Blackfield[a], E. Cook[a], S. Falabella[a], Ed. Gower[a],
J. Harris[a], S. Hawkins[a], B. Hickman[a], C. Holmes[a], A. Horner[a], S. Nelson[a],
A. Paul[a], D. Pearson[b], B. Poole[a], R. Richardson[a], D. Sanders[a], J. Stanley[a],
J. Sullivan[a], L. Wang[a], J. Watson[a], and J. Weir[a,c]

[a]*Lawrence Livermore National Laboratory, P.O. Box 808, L-641, Livermore CA, 94550, USA*
[b]*TomoTherapy, Inc., 1240 Deming Way, Madison WI 53717-1954, USA*
[c]*Compact Particle Acceleration Corporation, Madison, WI*

Abstract. Compact dielectric wall (DWA) accelerator technology is being developed at the Lawrence Livermore National Laboratory. The DWA accelerator uses fast switched high voltage transmission lines to generate pulsed electric fields on the inside of a high gradient insulating (HGI) acceleration tube. Its high electric field gradients are achieved by the use of alternating insulators and conductors and short pulse times. The DWA concept can be applied to accelerate charge particle beams with any charge to mass ratio and energy. Based on the DWA system, a novel compact proton therapy accelerator is being developed. This proton therapy system will produce individual pulses that can be varied in intensity, energy and spot width. The system will be capable of being sited in a conventional linac vault and provide intensity modulated rotational therapy. The status of the developmental new technologies that make the compact system possible will be reviewed. These include, high gradient vacuum insulators, solid dielectric materials, SiC photoconductive switches and compact proton sources. Applications of the DWA accelerator to problems in homeland security will also be discussed.

Keywords: Compact Dielectric Wall Accelerator, High Gradient
PACS: 41.90.+e

INTRODUCTION

DWA technology originated with a desire for more compact flash x-ray radiography sources [1]. Many of these flash x-ray radiography machines are linear induction accelerators with pulses that are tens of nanoseconds long. The typical accelerating gradient in the acceleration gap of a state of art induction cell is on the order of 10 - 20 MeV/m. However, the large magnetic cores used in the conventional induction accelerators lengthen the induction cells and lower the average accelerating gradients over the entire induction accelerators to the range of 0.3 – 0.5 MeV/m. To increase the average accelerating gradient, a coreless induction accelerator was introduced [2] in 1970. Its beam tube was made of an insulator, and the voltage across the insulator was supplied by transmission lines. This early dielectric wall accelerator demonstrated an average gradient of 1 MV/m for a 25-ns pulse, which was already higher than the gradient of contemporary linear induction accelerators.

The high gradient dielectric wall accelerator (DWA) system being developed at Lawrence Livermore National Laboratory (LLNL) [1,3-5] uses fast switched high voltage transmission lines to generate pulsed electric fields on the inside of an accelerator tube, which consists of many alternating fine layers of floating conductors and insulators. Compared to the conventional insulators, the conductor-insulator sandwich layer configuration, i.e., high gradient insulator (HGI) configuration, yields 2 – 5 times higher surface flashover threshold [6]. High electric field gradients on LLNL DWA are achieved by the use of HGI, short pulse times and "virtual traveling wave" operation mode [3,4]. The system is capable of accelerating any charge to mass ratio particle. The key components for such DWA are high gradient vacuum insulators, high bulk breakdown strength dielectrics for pulse forming lines [7], and closing switches compatible with operation at high gradient [8]. Currently we are developing a short pulse (~ 3 ns) compact proton therapy DWA system, which would fit in a conventional treatment vault [3-5, 9]. The proton DWA machine will deliver proton beams with energies in the range of 70 – 250 MeV. Extraction of protons from the source and focusing are accomplished electrically by adjusting pulsed voltages on various electrodes. Hence, the charge per bunch, spot size and beam energy can be varied on a pulse to pulse basis [9]. With the machine at about 50 Hz, the compact DWA proton machine can be used to provide intensity modulated proton therapy. We reported our work on high gradient dielectric wall technologies and a compact proton source for the compact DWA proton therapy project in References [3-5, 10]. In this paper we report on the recent progress in these areas. Progress in development of some accelerator architectures will also be presented. Finally, applications of the DWA accelerator to problems in homeland security will be discussed.
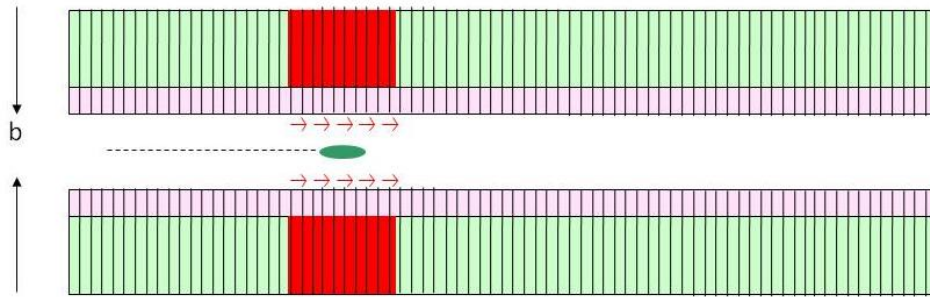

FIGURE 1. The vertical lines indicate the pulse forming lines that supply pulsed voltages across the HGI. The arrows along the HGI surface denote the longitudinal accelerating electric field of the virtual traveling accelerating voltage wave.

VIRTUAL TRAVELING WAVE DWA

The beam tube of the high dielectric wall accelerator is a stack of high gradient insulator, which is consistent of alternating layers of insulators and conductors. Characteristically, insulators' surface breakdown thresholds go up as the applied voltages' pulse width go down. To attain the highest accelerating gradients in the dielectric wall accelerator, the accelerating voltage pulses should only be on during the

shortest possible duration. Hence, along the HGI tube, the accelerating voltage should only be on locally when the charge particle bunch arrives. That fact suggests using DWA as a virtual traveling wave accelerator. Conceptually, the simplest architecture of the virtual traveling wave DWA is illustrated in Figure 1. Many pulse forming lines feed the continuous HGI tube. By timing the switches in each line, accelerating voltage pulses arrive at the accelerator axis along the beam tube at different times that appears to the charge particle bunch as a traveling accelerating voltage wave. By changing the timing, the virtual traveling wave can travel down the accelerator with the bunch with any charge to mass ratio. The HGI beam tube is capable of supporting a substantial tangential electric field. If the spatial extent of this electric field greater than 1.5 times of the beam tube diameter divided by the Lorentz factor γ, the on-axis field is comparable to the field along the wall [1]. Then the charged bunch will be accelerated by a large accelerating field. Note that the Lorentz factor increases as the beam being accelerated. Hence, to maintain the high on-axis accelerating electric field, the accelerating field's pulse width needs to be decreased as the beam gains energy.

FIRST ARTICLE SYSTEM TEST

Our goal is to fit the proton machine inside a conventional treatment room. To make the proton DWA accelerator compact requires five essential elements: high gradient insulators (HGI) with high surface breakdown strength, a pulse forming line architecture providing square pulses, fast switches with high bulk breakdown strength, large dielectrics with high dielectric constant and bulk breakdown strength, and a compact proton source capable of delivering sub-ns proton bunches. We are testing these components on the First Article System Test (FAST), a Blumlein accelerator system consisting of a stack of 1.83-cm high HGI and 7 Blumleins containing SiC photoconductive switches (shown in Fig. 1). Coupled directly into the HGI, all Blumeins are fired at the same time when the switches are illuminated with an expanded laser beam simultaneously. The FAST could be taken apart and rebuilt rapidly to increase system performance by using improved components.

Figure 1: First Article System Test outside and inside its oil tank

FAST as electron Diode

FAST was first operated as a diode with a flashboard cathode and a wire mesh at each end of the HGI. All 7 switches on the 7 Blumleins were fired simultaneously. The Blumleins impedance is about 40 Ohms. Beam loading from either the electron or proton beam on the FAST is negligible. Hence, the 3-ns output voltage across the HGI rang for several cycles (see Fig. 2). Figure 3 shows the FAST electron diode's Anode-Cathode gap voltage and electron current measured by the beam current monitor right after the exit of the Anode-Cathode gap and a Faraday cup further downstream. The data was taken with only one stack of Blumleins.
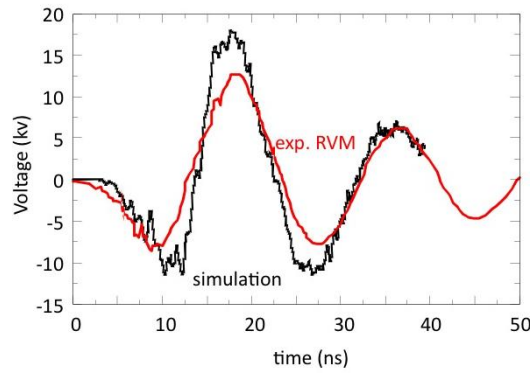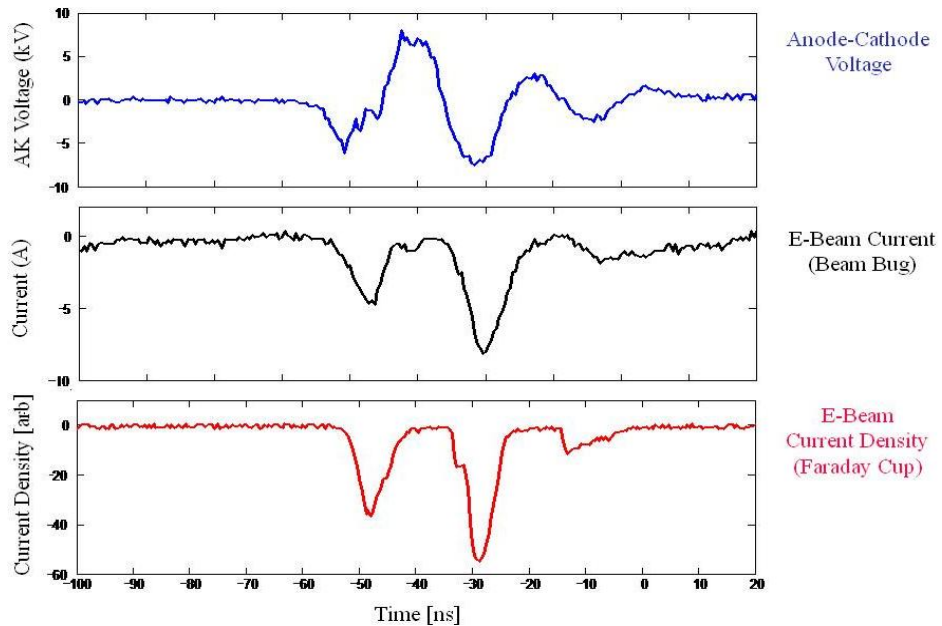
Figure 2. The FAST's accelerating voltage pulse

Figure 3. The FAST electron diode's A-K gap voltage and observed electron beam current. The electron current was extracted only when the Anode-Cathode voltage was negative.

Accelerating Field Waveform and Switches

As shown in Figure 4, FAST's accelerating field is sensitive to the switches' on-resistance, determined by the driving laser's power, the ability to get laser power into the switches, and the design and impurity properties of the switches. In Figure 5, the variance of the output pulse with the input optical pulse is shown. Note that the black curve shows an actual temporal laser pulse (mapped into conductivity space) while the other three curves show idealistic optical driving waveforms. For long pulses (> 3ns) the exact pulse shape is less important. For short pulses (< 2ns) the output is clipped since the system cannot fully drain the line before the switch has closed for Blumleins of this electrical length.
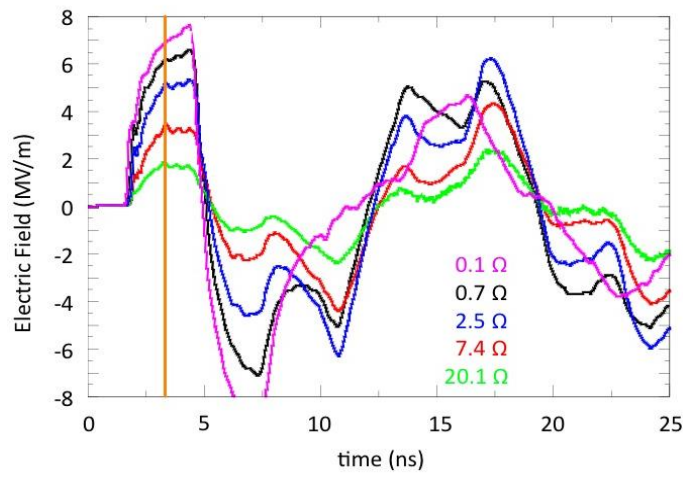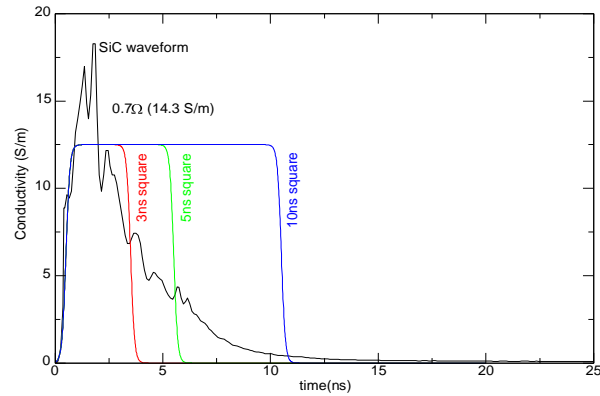
Figure 4. The FAST's on-axis accelerating field waveform with various SiC on-resistance.

Conductivity waveforms: black=SiC, red=3ns, green=5ns, blue=10ns

On-axis electric field in the middle of the stack including the
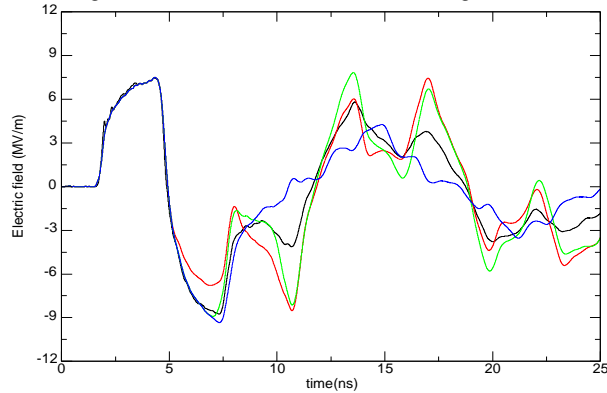20% geometric effect. Black=SiC, red=3ns, green=5ns, blue=10ns

Figure 5. Variance of the FAST accelerating field waveform with the laser optical waveform and pulse length. The initial pulse from the structure has the tightest fidelity (for pulse widths beyond 3ns). For optical pulses less than 2ns wide, the output pulse is clipped before it is able to reach the peak value (not shown).

SIC Photoconductive Switches

While the FR-4 solid dielectric in the FAST Blumeins was anticipated to be the electrical weak point, the switches had bulk breakdown due to structural defects. Our first SiC photoconductive wafers, from a different supplier, were free of these defects and exhibited bulk breakdown strength close to 250 MV/m. We have obtained new defect free SiC wafers from another source. The FAST photoconductive switches, measured 10mm x 10mm x 1 mm in size, were soldered into the pulse forming lines with circular electrodes on top and bottom. The switches were operated up to 30 kv charge voltage before breaking. Figure 6 shows the failed switches with burn marks around the edges of the electrodes. Each of the failures occurred at an electrode edge where the field stress was computed to be a maximum. The computed electric field stress for the configuration used in the experiments is shown in Figure 7 along with a schematic of the switch, electrodes, solder pads and oil. Due to the switch packing configuration, there is a factor of 10 field enhancement at the edges of the electrode. While the average field stress in the switches was about 30 MV/m, the field along the

conductive solder edge is about to 350 MV/m, which is in excess of the bulk breakdown strength of the material. This edge enhancement effect of switch packaging in the Blumeins limited FAST accelerating voltage to about 8 kV. Out present goal is developing an enhancement-cast-free, integrated switch package.

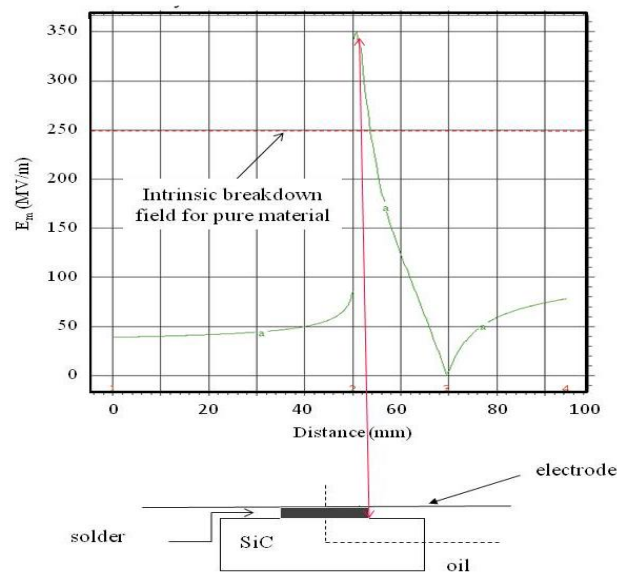Figure 6. Three failed SiC photoconductive switches with burn marks around the edges of the electrodes.

Figure 7. The computed electric field stress along the top surface of the SiC wafer and a schematic of the switch, electrodes, solder pads and oil.

Cast Dielectric Material

We are developing a cast solid dielectric material in the pulse forming lines to simplify the fabrication process and to reduce the cost. To supply an accelerating voltage for a given pulse length, the length of the pulse forming line is inverse proportional to the square root of the relative dielectric constant. For a compact DWA accelerator, it is desirable to have a material with a dielectric constant as large as possible. It would also be desirable to have a material whose properties can be varied for the applications. An earlier paper [4] reported that the material being developed at LLNL [4] having high dielectric constant nano-particles being mixed into an epoxy matrix. The effective dielectric constant of the material can be varied easily from 3 to 50 by adjusting the concentration of the nanoparticles. For low concentrations of the nano-particles, the bulk breakdown strength of the material under DC and pulsed conditions in these small samples is reported to be greater than 400 MV/m. Recently

we have tested larger pieces of cast dielectric material configured as 4 cm x 22 cm pulse forming lines. These samples consisted of the base material only, epoxy, without any nano-particle. One of these samples is shown in Figure 8. The separation between the two parallel electrodes is 0.8 mm. The electrodes are 0.127 mm thick and 1 cm wide with rolled edges and are embedded within the epoxy. This sample failed along the edge of an electrode at a pulsed voltage of 140 kV for an average field stress between the electrodes of 170 MV/m. The breakdown field stress versus accumulated number of shots along with the typical voltage trace used for the tests are given in Figure 9. Note that the charging waveform used in the test has a full width at half maximum greater than 300 ns. The charging waveform typically only needs to be 5 times of the electrical length of the Blumleins. For a 3ns output pulse, a 20ns charging waveform would be sufficient. These test cast dielectric samples in pulse forming line configuration have demonstrated capability of supporting a 100 MV/m machine gradient not only for the 3-ns proton therapy accelerator but also for long pulse machines with pulse length on the order of tens of nanoseconds.

Figure 8. A sample of cast dielectric material configured in a pulse forming line structure. The dark marks at the upper right edge of the electrode indicate where failure occurred.
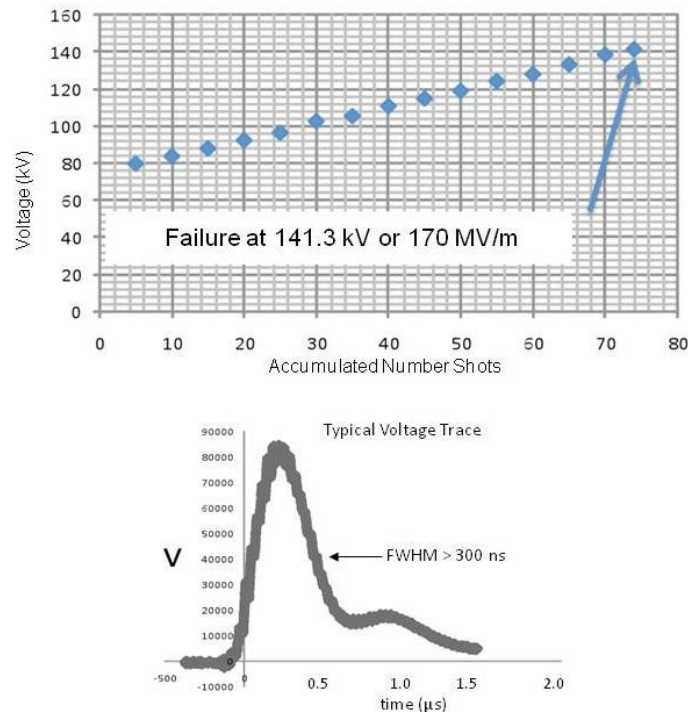

Figure 9. The breakdown field stress of the cast dielectric material in pulse forming line configuration versus the accumulated number of shots and the typical charging voltage waveform used for the test.

INJECTOR TEST STAND

Typical proton sources, such as ECRH source, used by the conventional proton accelerators are large and complex. To fit the compact DWA proton accelerator in a single treatment room requires a compact proton source. We are developing compact proton sources on our injector test stand. The compact proton source currently being investigated at LLNL, shown in Figure 10, is a two-strip spark source [4] operated with hydrogen loaded Ti and 4.7 kV, 175 ns, 60 A spark drive. The source is studied on the proton injector test with two configurations: standing alone and being mounted on the top of the FAST (see Figures 11 and 12 for on the top of the FAST). The spark plasma expands for 2.5 cm before the extraction grid. The spark and extraction grid are biased at +600 V. Following that is a grounded electron repelling grid. The gate grid was biased to +3.4 kV, blocking ion transport until the 20 ns FWHM, 10 kV gate pulse arrives. The region between the gate/anode grid and anode grid is a 3-cm A-K gap. An induction system consisting of 5 induction cells with 5 spark gap switched Blumleins provides the A-K gap voltage up to 250 kV, with a 30 ns rise time and no flattop, to ensure proton transit time in FAST shorter than 3 ns so protons would be accelerated while passing through FAST. The 10-keV proton's transient time through the 250-kV A-K gap is about 7 ns. For the injector mounted on the top of the FAST configuration, there is a 2.15-cm drift before FAST's entrance grid. The FAST DWA accelerator section is terminated with a grid.
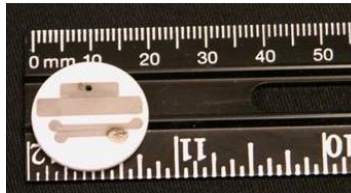

Figure 10. A spark source consists of two hydrogen-loaded Ti Strips

Diagnostics

An ion collector with entrance grid is located 15.7 cm downstream of the DWA exit grid. An 1-mm (2mm) aperture in the ion collector's entrance grid allows passage of ions into a slit collimator (0.25 mm x 1.5 mm with 62 mm separation) at the entrance to the Thomson spectrometer. This choice gives a proton energy resolution of a few keV, with less concern for the mass resolution. Permanent magnets with $\int B \cdot dl = 18$ kG-cm and a variable electric field deflected the ions. 17.3 cm from the magnet center, a micro-channel plate with phosphor anode was used for ion detection. Images were recorded by a camera with gated intensifier.

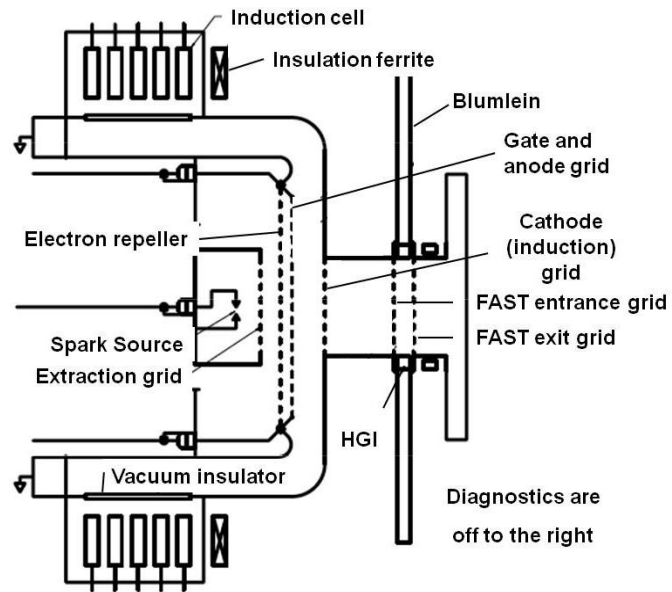Figure 11. Proton injector and FAST test stand.

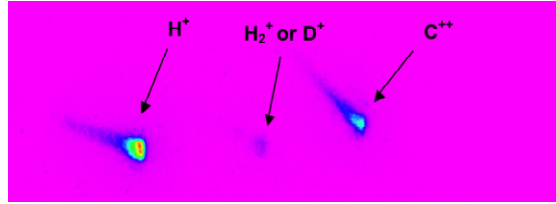Figure 12. Layout of proton injector and FAST.

Figure 13. Typical Thomson spectrometer image. Position of undeflected axis is off the right side of the image. Long dimension of slit is vertical in this image. Magnetic deflection is to the left, and electric deflection is upward in the image.

Results

Typical Injector Behavior with a Hydrided Titanium Source

A proton current of a few mA is typically observed on the ion collector. Prior to energizing the FAST DWA module, the full mass spectrum was recorded with the Thomson spectrometer. A typical spectrum is shown in Fig. 13, with an inductive acceleration of 210 kV. The spectra are consistent with the normalized mass to charge ratios, m/q, being 1, 2, and 6, which are interpreted as H^+, D^+, and C^{2+}. Hydrogen, bound atomically to the Ti surface in the spark source, is released during the spark and then ionized. Without a hydrogen gas fill, few molecular ions are expected [12]. The ion signal at m/q = 2 is less than 10% of the H^+ signal, but significantly above the 1.2e-4 fraction of naturally occurring deuterium. It is possible due to deuterium contamination of the source Ti, since the hydrogen loading of Ti for this source was performed after the system was used to load deuterium for a D^+ source. Currently Other tests were performed to determine if that is the cause of the m/q = 2 signal. The test results are reported later in the section on a deuterated titanium source. Depending on the timing between the arc voltage and the gate pulse, different species of ions are extracted. When the gate voltage is pulsed early, only the fastest ion species, i.e., protons reach the gate when the gate is open, and hence, pure protons are extracted. Since the characteristic of the transient plasma is sensitive to the details of arcing, such as the location of arcing, the shape of electrode at that location, etc., the extracted proton currents are not quite repeatable. Ion extraction is reasonably repeatable when the gate voltage is pulsed after the bulk of plasma has arrived at the gate. However, many heavier ion species, such as C++ or D+ are also extracted. To minimize the heavier ion impurities, the gate is pulsed early to capture the leading edge of the spark plasma. Acceleration of the C^{2+} ions in the injector and by the FAST is small due to their long transit times across the A-K gap and the FAST DWA structure plus the late arrival time at the FAST. Ions with larger m/q, such as OH^+ and C^+, are not accelerated as their transit time across the A-K gap is longer than the duration of the induction accelerator pulse, which may explain why they are not observed.

Acceleration by FAST

Based on the FAST timing, protons could be accelerated or decelerated. Calculations of proton energy after FAST are given in Figure 14. For each FAST voltage, energies for the timing set to (a) accelerate and (c) decelerate protons, and (b)

no FAST pulse are plotted. The multiple values of beam energy at a given time are due to protons' catching up or slipping along the beam pulse. Energy modulation introduced by the 8-kV FAST's timing can be easily observed with either time resolved or integrated energy diagnostics. In Figure 15, the region of the Thomson spectra proximate to the H^+ is shown, and the effect of energizing FAST is easily observed. The timing of FAST was set such that proton energies were increased or decreased as shown. The peak energy shift is consistent with the integrated FAST voltage waveform over a proton transit time at this injection energy as is the relative width of the energy spectra for the 3 cases (compare with Fig. 13a). Simulated charge versus energy results by using a 3D electromagnetic particle-in-cell code, LSP, are also shown in Figure 15. The measured energy spectra agree with the simulated result quantitatively.
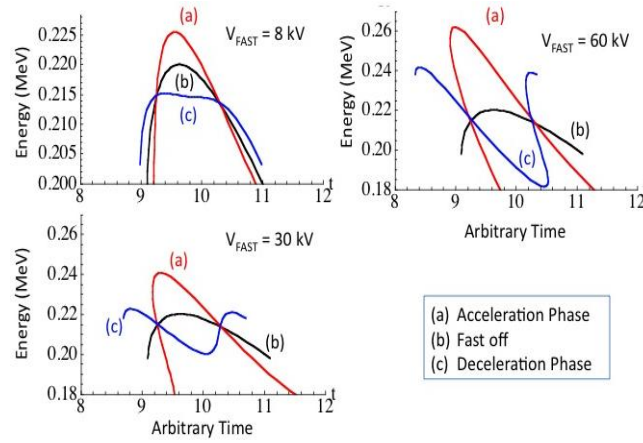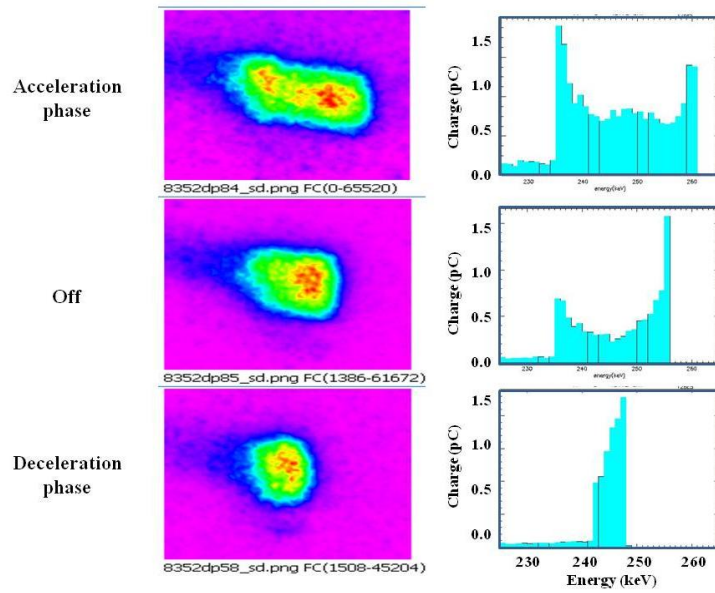

Figure 14. Proton energy after FAST.

Figure 15. Thomson spectrometer images around H^+ and the simulated charge versus energy when FAST is energized and phased to accelerate/decelerate protons or FAST is off.

Operation with a Deuterated Titanium Source

To determine the origin of the m/q = 2 ions during hydrided source operation, a deuterated titanium source was installed. If the m/q = 2 signal in Figure 13 was due to molecular hydrogen ions, an m/q = 4 signal would now be expected. Note than C^{3+} also has m/q = 4, so care must be taken with data interpretation, and some ambiguity will remain. Figure 16 shows an image from the Thomson spectrometer when the gate is pulsed moderately early, but after the leading edge of the spark plasma. At this gate time, there are 4 ion species present, including one at m/q = 4. It is worth noting that m/q = 4 was not observed without m/q=3 also present, suggestive that it is indeed C^{3+}. However, if the gate is pulsed later in the source plasma expansion, no C^{3+} is observed, see Figure 17. If there were a mechanism for molecular ion production, one would expect it to be more likely to occur during the later, cooler times of the source spark. Those molecular ions would then arrive at the extraction grid later, rather than earlier as is observed here. Circumstantially then, it appears most likely that there are no molecular hydrogen ions observed from the spark source.
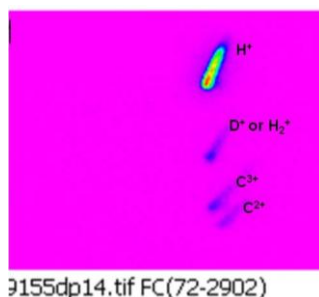

Figure 16. Thomson spectrometer image from deuterated titanium source. To enhance species visibility, the induction cells were deliberately mistimed to give a larger than normal energy spread to the ions.
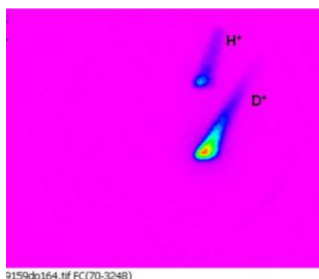

Figure 17. Thomson spectrometer image from deuterated titanium source, gate pulsed later in source expansion than Figure 16.

Finally, Figure 18 shows the relative amounts of H+ and D+ as the gate pulse time is varied with respect the to the spark initiation time for two different spark energies. The later arrival of the D^+ relative to the H^+ and the increase of only the D+ with spark energy suggests that the H+ comes only from surface contaminants whereas the D+ is thermally desorbed from the deuterated Ti. This provides a bit of a counterpoint to the

hypothesis in the previous section, given the likelihood that the process for H liberation (from surface) is different from that for D (from deeper in Ti).
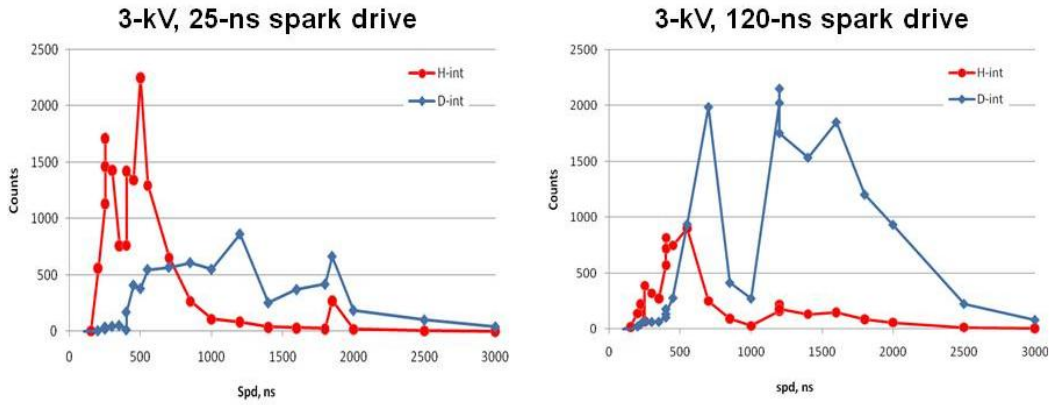

Figure 18. Relative counts of H+ and D+ as the gate delay from spark initiation is varied. a) 3 kV, 25 ns spark drive, b) 3 kV, 120 ns spark drive.
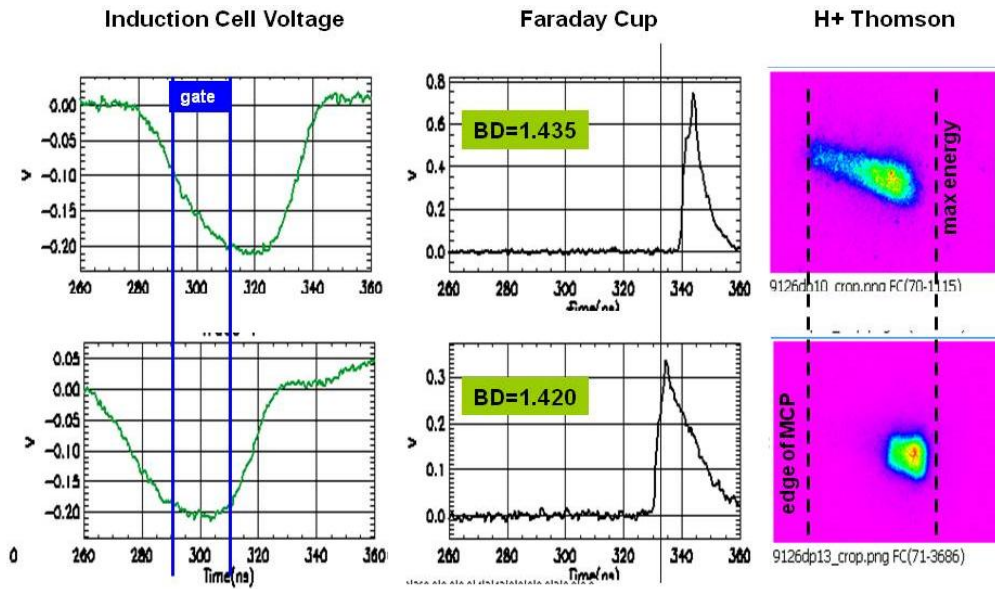

Figure 19. Induction cell voltage waveform, proton current collected by a Faraday cup and Thomson spectra as gate pulse time is varied. The gate time is indicated on the induction cell voltage waveforms. Thomson spectrum shows a large energy spread for the case with a large energy ramp.

4. Temporal beam compression of a proton beam:

By pulsing the gate during the rise time of the induction cells, an energy ramp can be applied to the accelerated protons. Voltage waveforms and collected ion currents for such a case are compared with those for nominal timing in Figure 19. For the top case, an energy ramp is applied. Longitudinal drift compression occurs, and, a compression of approximately 2 was observed in the proton pulse width at the location of the ion collector.

ACCELERATOR ARCHITECTURE

On the surface using a stack of pulse forming lines to supply the accelerating voltage to the HGI beam tube is straightforward. Unfortunately, the current flowing inside a pulse forming line would create a magnetic field, which wraps around the neighboring lines and causes unwanted parasitic coupling. The end result is low voltage output and poor waveform. One way to eliminate the parasitic coupling inside a stack of pulse forming line is to use conventional induction cells to supply the accelerating voltage instead, as shown in Figure 20. Photoconductive switches are placed along the continuous HGI tube. The HGI tube with switches functions like a voltage adder stalk. When all the switches are turned on by laser lights except one, the sum of the voltage from all the induction cells appears across that off-switch, which becomes an acceleration gap to the beam. By adjusting the switch timing, this accelerator configuration can be operated in the virtual traveling wave mode described earlier in the paper for any type of charge particle beam. While the gradients in the induction cells are low, the gradient across the gap could be orders of magnitude higher. One can imaging building a meter long 1-MeV induction machine. Assume the dimension of a photoconductive wafer is 1 cm along the machine axis. Ignoring the fringe field, the field gradient in the virtual acceleration gap across the open switch is 100-MeV/m. By adjusting the switch timing, an accelerator with this configuration could potentially deliver a 100-MeV beam.
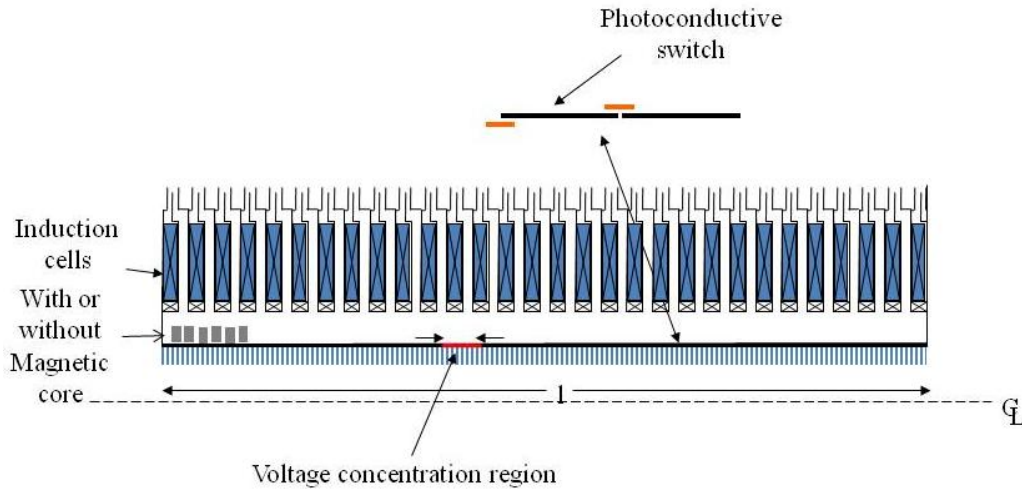

Figure 20. The virtual traveling wave DWA inductive adder configuration.

The voltage adder effects in the virtual traveling wave DWA inductive adder configuration is modeled with a 3-D electromagnetic code, XFDTD. The simulated inductive adder consists of 23 inductive cells, shown in Figure 21 along with their magnetic cores. Each cell provides 1 Volt to the system. The switch tube consists of 10 6-cm switch segments. Each segment is presented in a different color in Figures 21 and 22. The tube's inner radius and outer radius is 2 cm and 2.5 cm, respectively. The temple profiles of photoconductive switches' conductivity used to simulate the switches being opened one by one are given in Figure 22(a). The simulated on-axis accelerating fields are shown in Figure 22(b). As discussed in the "Virtual Traveling

Wave DWA" section and in Ref. [1], the spatial extent of the electric field on the switch tube wall needs to be greater than 1.5 times of the tube diameter divided by the Lorentz factor γ in order to have the on-axis field comparable to the field along the wall. In the simulation, the 1-cm switch segment length is much less than 1.5 times of the switch tube's inner diameter. Therefore, the fringe field is large and the on-axis field is much weaker than the field along the wall in the virtual gap region. However, Figure 21(b) still demonstrates successfully the effects of voltage concentration in the virtual moving gap.
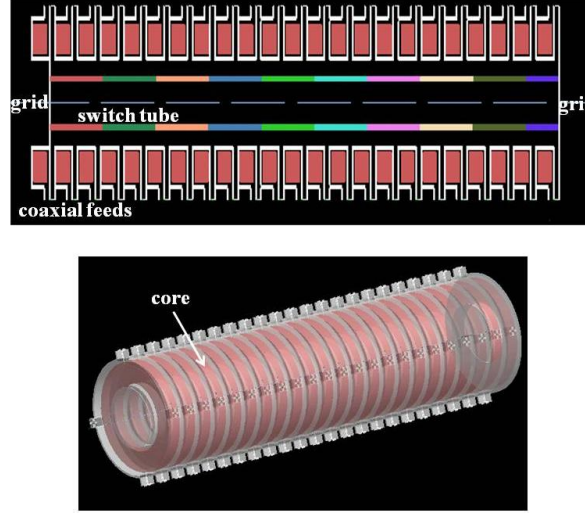

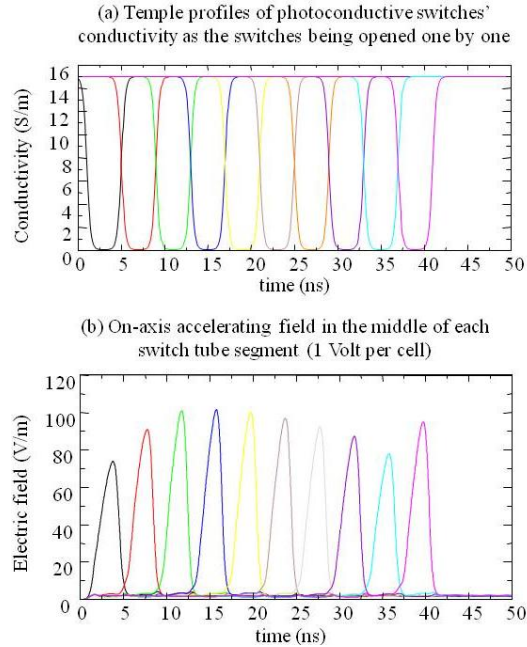Figure 21. The virtual traveling wave DWA inductive adder configuration used in the XTDFD simulation.

Figure 22. (a) Temple profiles of switches' conductivity and (b) simulated accelerating field in the virtual traveling gaps.

HOMELAND SECURITY APPLICATIONS

As mentioned in the introduction, the high-gradient dielectric wall technology was originated by the desire of having compact flash x-ray radiography source. While the machine becomes small, the DWA radiography sources will also become transportable and cheaper. Hydro tests could then be done at various sites instead of at a fixed facility. Potentially, one can also use several DWA radiography sources to take radiographic photos of objects from several lines of sight at the same time.

There are many other potential applications of the high-gradient dielectric wall technology for homeland security needs. One of these applications is to provide an active interrogation source on a mobile platform for special nuclear material detection from a standoff distance. For example, using an DWA to provide a 1 − 4 GeV proton beam. Depending on the dose specifications, the compact DWA proton therapy accelerator's pulse format potentially is also suitable for proton interrogation. Then, the proton therapy machine could be used as the front end of the GeV proton interrogation machine. The DWA technology can also be used as a driver for muon beam by produce proton beam, which is then used to produce muon beam for muon probe. Similarly, A DWA electron accelerator can provide an electron beam for production of tunable gamma ray beam. Figure 23, taken from ref. [6], shows the observed vacuum surface breakdown strength for high-gradient-insulators and various conventional insulators as functions of the pulse width of the applied electric field. The data indicate that HGI can sustain an electric field stress at least 2 to 5 times higher than what the conventional insulator can. The HGI data suggests a wide range of choices for the accelerating field gradient and pulse length. For example: the accelerating field in a DWA accelerator could be 100 MV/m with a 3 ns pulse width or at 30 MV/m with 200 ns pulse. The optimal pulse length, accelerating field gradient and charge per bunch would be determined by the applications.
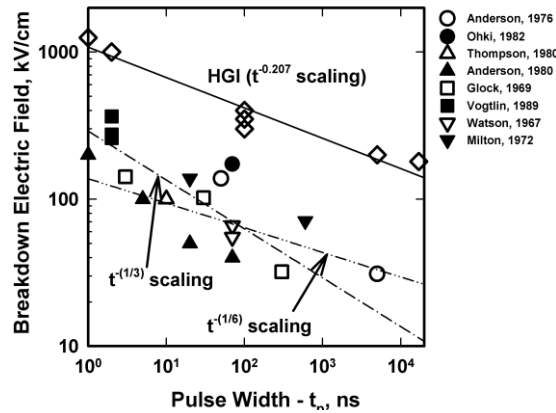

Figure 23. Comparison of multilayer HGI structures with conventional 0° insulators [6].

CONCLUSIONS

The high gradient dielectric wall technology promises to increase the accelerating gradient of high current accelerators dramatically. Good progress is being made on all the important DWA elements. The FAST has demonstrated acceleration of electrons and protons successfully. With a 300 ns FWHM charging voltage pulse, the cast dielectric material in a pulse forming line configuration holds a field stress to up to 170 MV/m. A spark source is being investigated for the potential compact proton source for the proton DWA for cancer treatment. We have described a new accelerator configuration, the virtual traveling wave induction concentrator. Finally, we have discuss some potential applications for homeland security missions.

ACKNOWLEDGMENTS

References

1. G. Caporaso, "New Trends in Induction accelerator Technology", Proceeding of the International Workshop on Recent Progress in Induction Linacs, Tsukuba, Japan, 2003.
2. A. I. Pavlovski, et. al., *Sov. At. En.* **28**, p. 549 (1970).
3. G. Caporaso, et. al., *Nucl. Instr. and Meth. in Phys. B* **261**, p. 777 (2007); www.sciencedirect.com.
4. G. Caporaso, et. al., "High Gradient Induction Accelerator", PAC'07, Albuquerque, June 2007, TUYC02, p. 857 (2007); http://www.JACoW.org.
5. G. Caporaso, et. al., "Status of the Dielectric Wall Accelerator", PAC'09, Vancouver, Canada, May 2009, TH3GAI02, (2009); http://www.JACoW.org.
6. S. Sampayan, et. al., *IEEE Trans. Diel. and Elec. Ins.* **7** (3) p. 334 (2000).
7. D. A. Sanders, et. al., "Development of a low loss, high dielectric strength microwave substrate", 27th Power Modulator Symposium, p. 291 (2006).
8. J.Sullivan and J. Stanley, "6H-SiC Photoconductive Switches Triggered Below Bandgap Wavelengths", Power Modulator Symposium and 2006 High Voltage Workshop, Washington, D.C. 2006, p. 215 (2006).
9. Y.-J. Chen and A. C. Paul, "Compact Proton Accelerator for Cancer Therapy", PAC'07, Albuquerque, June 2007, TUPAS059, p. 1787 (2007); http://www.JACoW.org.
10. Y.-J. Chen, et. al., "Compact Proton Injector and First Accelerator System Test for Compact Proton Dielectric Wall Cancer Therapy Accelerator", PAC'09, Vancouver, Canada, May 2009, TU6PFP04, (2009); http://www.JACoW.org.
11. S. Falabella, et.al., "Characterization of a Surface-Flashover Ion Source with 10-250 ns Pulse Widths", Proc. of the 12th CAARI, March 2009, Vol. 1099, p. 99 (2009).
12. E. Cheifetz, U. Adar, and G. Davara, Proc. 17th International Symposium on Discharges and Electrical Insulation in Vacuum, Berkeley, p194 (1996).